THE JOURNAL OF BIOLOGICAL CHEMISTRY VOL. 290, NO. 12, pp. 7930–7942, March 20, 2015

Quantifying Ca^{2+} Current and Permeability in ATP-gated P2X7 Receptors*

Received for publication, November 21, 2014, and in revised form, January 27, 2015 Published, JBC Papers in Press, February 2, 2015, DOI 10.1074/jbc.M114.627810

Xin Liang (梁欣)[‡], Damien S. K. Samways[§], Kyle Wolf[¶], Elizabeth A. Bowles[‡], Jennifer P. Richards[‡], Jonathan Bruno[‖], Sébastien Dutertre[**], Richard J. DiPaolo[¶], and Terrance M. Egan[‡1]

*From the [‡]Department of Pharmacological and Physiological Science and Center for Neuroscience, and the Departments of [¶]Molecular Microbiology and Immunology and [‖]Internal Medicine, Saint Louis University School of Medicine, St. Louis, Missouri 63104, the [§]Department of Biology, Clarkson University, Potsdam, New York 13699, and the **Institut des Biomolécules Max Mousseron, UMR 5247, Université Montpellier 2, CNRS, Montpellier, France*

Background: Ca^{2+} triggers many of the actions of extracellular ATP.
Results: We measured the Ca^{2+} component of the ATP-gated non-selective cation current of P2X7 receptors.
Conclusion: Ca^{2+} flux varied with the species of origin, the splice variant, and the agonist concentration.
Significance: Our results suggest that domains that lie outside of the pore regulate the Ca^{2+} flux of P2X7 receptors.

ATP-gated P2X7 receptors are prominently expressed in inflammatory cells and play a key role in the immune response. A major consequence of receptor activation is the regulated influx of Ca^{2+} through the self-contained cation non-selective channel. Although the physiological importance of the resulting rise in intracellular Ca^{2+} is universally acknowledged, the biophysics of the Ca^{2+} flux responsible for the effects are poorly understood, largely because traditional methods of measuring Ca^{2+} permeability are difficult to apply to P2X7 receptors. Here we use an alternative approach, called dye-overload patch-clamp photometry, to quantify the agonist-gated Ca^{2+} flux of recombinant P2X7 receptors of dog, guinea pig, human, monkey, mouse, rat, and zebrafish. We find that the magnitude of the Ca^{2+} component of the ATP-gated current depends on the species of origin, the splice variant, and the concentration of the purinergic agonist. We also measured a significant contribution of Ca^{2+} to the agonist-gated current of the native P2X7Rs of mouse and human immune cells. Our results provide cross-species quantitative measures of the Ca^{2+} current of the P2X7 receptor for the first time, and suggest that the cytoplasmic N terminus plays a meaningful role in regulating the flow of Ca^{2+} through the channel.

All P2X receptors transduce a significant Ca^{2+} flux at the resting membrane potential (1) that triggers many of the physiological and pathophysiological actions of extracellular ATP (2–6). The molecular physiology of the Ca^{2+} flux is poorly understood despite outstanding recent advances in functional and structural studies (7). This is particularly true for the P2X7 receptor (P2X7R) that is unusually sensitive to allosteric block by extracellular Ca^{2+} (8), a fact that makes characterization of the Ca^{2+} component of the ATP-gated current particularly problematic (9, 10).

P2X receptors are a family of seven ATP-gated ion channels (P2X1R–P2X7R) that subserve a diverse range of functions in a subunit selective manner. The prominent expression of P2X7Rs in lymphocytes, macrophages, and microglia (11–14) suggests a vital role for this subtype in the immune response (15). P2X7Rs are inactive in healthy tissue because limited release and rapid hydrolysis keep the concentration of extracellular ATP ($[ATP]_o$) low (<100 nM) (16–18). However, the $[ATP]_o$ rises to millimolar concentrations at sites of stress, cellular injury, tumor necrosis, and phagocytic degranulation (16, 18–21) where it acts as a "danger" signal that initiates innate immunity by stimulating the caspase-1-activating platform known as the "inflammasome" (22–24). The result is an increased production and rapid release of pro-inflammatory cytokines by mononuclear phagocytes (15, 24–26), ultimately leading to greater inflammation and/or cell death (13, 15). In many cases, the inward flow of Ca^{2+} through the P2X7R is a key component of this response (28–30). Furthermore, the sustained rise in the intracellular concentration of free Ca^{2+} that follows activation of P2X7Rs directly triggers macrophage apoptosis independent of pro-inflammatory signaling cascades (31).

P2X7Rs are also expressed by neurons and glia of the peripheral and central nervous systems (5) where they influence differentiation, homeostasis, and disease in part by increasing intracellular Ca^{2+} (25, 32–36). In the peripheral nervous system, the elevated $[ATP]_o$ that accompanies inflammatory bowel disease leads to rapid degeneration of gut neurons by direct activation of the P2X7Rs of the myenteric plexus (37). In the eye, subretinal hemorrhage increases the $[ATP]_o$, leading to a P2X7R-dependent Ca^{2+} influx that activates caspase-8 and initiates photoreceptor cell apoptosis (38). In the central nervous system, P2X7Rs are found on microglia, oligodendrocytes, and astrocytes, where they contribute to the genesis of neuropathic and chronic inflammatory pain (25) and influence cell survival (39). Although the presence of P2X7Rs on central neu-

* This work was supported, in whole or in part, by National Institutes of Health Grant HL56236 (to T. M. E.) American Cancer Society Research Scholar Grant 12-171-01-LIB (to R. J. D.), and Blue Ribbon Funding from the St. Louis University School of Medicine (to T. M. E.).

This paper is dedicated to the memory of Thomas H. Steinberg, M.D. (1952–2013), who was a true pioneer in the study of ATP-gated P2X7Rs.

[1] To whom correspondence should be addressed: 1402 South Grand Blvd., St. Louis, MO 63104. Tel.: 314-977-6429; Fax: 314-977-6411; E-mail: egantm@slu.edu.

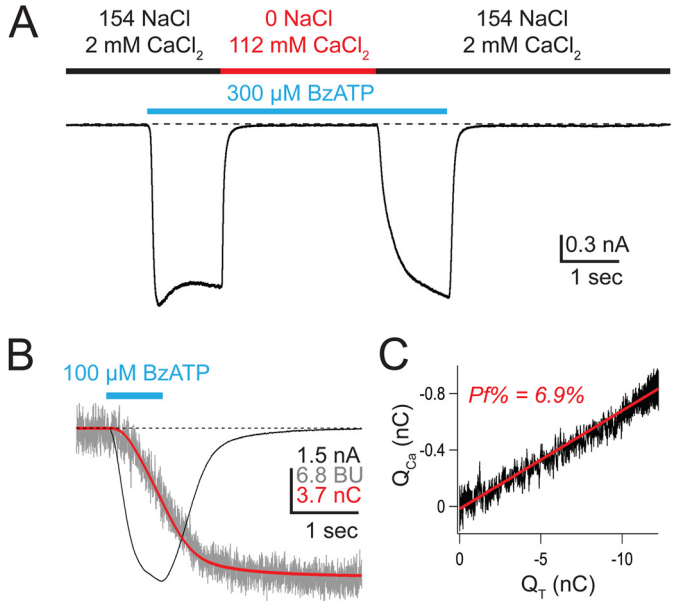

FIGURE 1. **Measuring the Ca^{2+} current of rat P2X7aR.** *A*, the inward current evoked by a supra-maximal concentration (EC_{50} = 20 μM (87)) of BzATP (*cyan bar*) is blocked in high extracellular Ca^{2+}. BzATP was applied first in an extracellular solution containing predominately NaCl (*black bar*), followed immediately by an extracellular solution containing predominately $CaCl_2$ (*red bar*). The high $[Ca^{2+}]_o$ completely blocks the BzATP-gated current. The current quickly recovers upon reintroduction of the NaCl solution. *B*, shows the BzATP-gated membrane current (*black trace*, in nA), the change in F_{380} (*gray trace*, in bead units), and the integrated current (*red trace*, equal to Q_T, in nC). *C*, Q_{Ca} (calculated from F_{380}; see "Experimental Procedures") is plotted against Q_T. The result is a straight line (slope = *Pf*), demonstrating that the change in fluorescence results entirely from Ca^{2+} entering through the channel (50). *BU*, bead units.

rons is controversial (6, 40), recent data suggest they play a role in modulation of release of transmitters and hormones (41, 42). For example, ATP-gated Ca^{2+} influx through presynaptic P2X7Rs triggers glutamate release from cortical synaptosomes (43, 44), GABA release from hippocampal slices (45), and arginine-vasopressin release from neurohypophysial terminals (46).

In this paper, we provide a quantitative measure of the Ca^{2+} component of the P2X7 current. The usual means of achieving this goal is to determine the permeability of Ca^{2+} relative to a reference monovalent cation (47). Unfortunately, measurement of relative Ca^{2+} permeability typically requires a high concentration (10–112 mM) of extracellular Ca^{2+} ($[Ca^{2+}]_o$) that blocks the rat P2X7 current (Fig. 1*A*) with an IC_{50} of ~3 mM (9, 48). To circumvent this problem, we used the dye-overload method to measure the percent fractional Ca^{2+} current (*Pf*%)[2] of the ATP-gated response determined in the presence of less than 2 mM free $[Ca^{2+}]_o$ (49, 50). The *Pf*% method has distinct advantages over traditional reversal potential measurements of permeability; it is a direct and model-independent measure of Ca^{2+} entry obtained using physiological concentrations of extracellular ions (51–53). By contrast, reversal-based techniques do not measure the physiologically relevant Ca^{2+} current, require high concentrations of extracellular Ca^{2+}, and make the tenuous assumption that the Ca^{2+} current follows the assumptions of the Goldman-Hodgkin-Katz equation (54, 55).

[2] The abbreviations used are: *Pf*%, percent fractional Ca^{2+} current; BzATP, benzoyl-ATP; NMDG, *N*-methyl-D-glucamine.

We measured the *Pf*% of an array of recombinant and native P2X7Rs, and found an unexpected variability in the contribution of Ca^{2+} to the total ATP-gated membrane current. The variability was most pronounced in the zebrafish P2X7R and in splice variants of murine P2X7Rs. Ten splice variants (P2X7bR–P2X7kR) have been identified from a range of species since the initial molecular cloning of the first P2X7R from rat (now called rat P2X7aR) (6). Only two of these (human P2X7bR and murine P2X7kRs) form functional homomeric receptors (56, 57). We discovered that mouse and rat splice variants with identical pore-lining sequences show significantly different *Pf*%, suggesting that domains that lie outside of the channel pore regulate the Ca^{2+} component of the ATP-gated current.

EXPERIMENTAL PROCEDURES

Human and animal procedures were approved by the Institutional Review Board and the Institutional Animal Care and Use Committee, respectively, of the St. Louis University School of Medicine.

Isolation of Human Macrophages—Monocyte-derived macrophages were obtained as described by Norenberg *et al.* (58). Blood obtained from healthy volunteers was centrifuged at 500 × *g* for 10 min to isolate plasma, buffy coat layer, and erythrocytes. The buffy coat layer was removed, diluted 2:1 with cold physiological buffered saline (PBS) with no added divalent cations, and then overlaid on 15 ml of Histopaque 1077 (Sigma) in a 50-ml centrifuge tube. The tube was centrifuged at 900 × *g* for 30 min to produce an interfacial layer of mononuclear cells, and platelets were isolated and then processed through three PBS wash and spin (250 × *g* for 7 min) cycles. After the final spin, the pelleted cells were resuspended in 8 ml of a culture medium made of SensiCell™ RPMI 1640, 7.5% heat-inactivated autologous plasma, 100 units/liter of penicillin, and 100 μg/ml of streptomycin (all from Life Technologies). The cell suspension was then divided equally among eight 4-well plates previously loaded with circular 13-mm glass coverslips (Gold Seal Cover Glass, Thermo Scientific, Waltham, MA), and placed in a humidified 5% CO_2 incubator for 2 h. Subsequently, the plates were washed several times with warm PBS to remove non-adherent cells, and the remaining cells were cultured in 0.5 ml of the culture medium for 6–14 days. Lipopolysaccharide (1 μg/ml, Sigma) was added for 6–12 h immediately preceding the start of the experiments.

Isolation of Mouse Macrophages—Peritoneal macrophages were obtained with modifications as described by Davies and Gordon (59). Two or three adult mice were intraperitoneally injected with 1 ml of sterile 3% Brewers thioglycoate (Thermo Scientific) using a 25-gauge needle. Four days later they were sacrificed via carbon dioxide inhalation and cervical dislocation. The abdominal skin was soaked with 70% ethanol, pulled up with sterile forceps, and cut to expose the peritoneal cavity. The peritoneum was injected with an ice-cold high-glucose Dulbecco's modified Eagle's medium (DMEM; with added glutamine and sodium pyruvate) (Life Technologies) using a 20-gauge needle, and the mouse was vigorously shaken for a few seconds. The suspended cells were then harvested by removing the DMEM from the peritoneal cavity using a 25-gauge needle. The cell suspensions obtained from individual mice were

pooled, and the cells were pelleted by centrifugation (5 min at 200 × *g*). The cell pellet was resuspended in 5 ml of cold Red Cell Lysis Buffer (Sigma), incubated for 5 min at room temperature, and then repelleted. The supernatant was discarded, and the remaining cells were resuspended in DMEM, 10% heat inactivated fetal bovine serum (FBS; Thermo Scientific), and non-essential amino acids (Sigma). The cells were plated at a density of 500,000 cells/35-mm tissue culture dish and cultured in a humidified 5% CO_2 incubator for up to 14 days. Two days before the experiment, the cells were replated onto 13-mm glass coverslips. Lipopolysaccharide (1 μg/ml) was added for 6–12 h immediately preceding the start of an experiment.

Isolation and Activation of Mouse Lymphocytes—Peripheral lymph nodes were isolated from BALB/c-FoxP3eGFP reporter mice (60). T cells were enriched using the Pan T cell isolation kit and AutoMACS magnetic bead separation (Miltenyi BioTech, San Diego, CA). Recovered T cells were stained for CD4-PE (clone GK1.5, BD Pharmingen) and purified by fluorescence activated cell sorting (FACS) to isolate $CD4^+FoxP3eGFP^+$ and $CD4^+FoxP3eGFP^-$ populations. To activate cells, 1.5×10^5 $CD4^+FoxP3eGFP^+$ and 2.5×10^5 $CD4^+FoxP3eGFP^-$ purified T cells were cultured in complete RPMI medium (2 mM glutamine, 1:100 non-essential amino acids, 1 mM sodium pyruvate, 10 mM HEPES, 100 units/ml of penicillin and streptomycin, 50 μM 2-mercaptoethanol, final concentrations) supplemented with 10% FBS and 100 units/ml of recombinant human interleukin-2 (rhIL-2). T cells were activated using plate-bound αCD3 (1 μg/ml) and αCD28 (2 μg/ml). *Pf*% was measured 24–72 h post-activation.

Culture and Transfection of HEK293 Cells—Standard methods of transfection and cell culture were used to express genes in HEK293 cells, as previously described (61, 62). HEK293 cells were maintained in exponential growth in Dulbecco's modified Eagle's medium supplemented with 10% heat-inactivated FBS, 2 mM glutamine, 50 units/ml of penicillin G, and 50 μg/ml of streptomycin, and incubated at 37 °C in a humidified atmosphere with 5% CO_2. The cells were enzymatically dissociated upon reaching 70–80% confluence in 75-cm^2 tissue culture flasks, and co-transfected with a P2X7R plasmid (2 μg) and a fluorescent reporter gene (0.5 μg) using Effectene (Qiagen, Valencia, CA). They were then replated in 35-mm culture dishes, and left to grow for 48 h before use in experiments. A 1:3 ratio of genes encoding the human P2X7aR (2 μg) and P2X7bR (6 μg) splice variants were used in co-expression experiments.

Imaging Ca^{2+} in a GCaMP5G Cell Line—HEK293 cells stably expressing GCaMP5G and transiently expressing AsRed were plated on glass coverslips for investigation using a fluorescent imaging system. GCaMP5G fluorescence was imaged using a CoolSnap EZ camera (Photometrics, Tucson, AZ) and the appropriate filter cube (excitation 480 nm; emission 510 nm). Imaging data were analyzed using μManager 1.4 (63).

Measuring Pf%Detailed descriptions of our method are described elsewhere (1, 62). Briefly, agonist-gated current (*black trace* in Fig. 1*B*) was measured electrically and then integrated (*red trace* in Fig. 1*B*) to give the total charge transfer across the cell membrane (Q_T, in coulombs). At the same time, Ca^{2+} influx was monitored from the fluorescence emitted by a high concentration (2 mM) of intracellular fura-2 K_5 (*gray trace* in Fig. 1*B*) introduced through the recording electrode. When all of the Ca^{2+} entering the cell was captured by the dye, then the change in 510 nm emission of fura-2 excited by 380 nm light (ΔF_{380}) was proportional to the Ca^{2+} flux through the pore (64). The ΔF_{380} signal was measure in bead units and calibrated in separate experiments as previously described (1), allowing ΔF_{380} to be converted to coulombs of Ca^{2+} charge (Q_{Ca}). Then, the fraction of total membrane current carried by Ca^{2+} (*Pf*) equaled Q_{Ca}/Q_T (slope of the line in Fig. 1*C*), and the percent fractional Ca^{2+} current (*i.e.* the *Pf*%) equaled $P_f \times 100\%$. In most cases, Q_{Ca} was a linear function of Q_T for the enter length of the ATP response, demonstrating that all of the incoming Ca^{2+} was captured by fura-2. Data showing non-linearity were discarded. The intracellular solution contained (in mM): 140 CsCl, 10 TEA-Cl, 10 HEPES, pH 7.3, with CsOH. The extracellular solution contained: 150 NaCl, 2 $CaCl_2$, 1 $MgCl_2$, 10 glucose, 10 HEPES, pH 7.4, with NaOH. $MgCl_2$ was omitted from the extracellular solution when 600 μM BzATP was used as agonist. Often, we were able to record several currents (2–10) from a single cell. In these cases, successive applications were separated by >2 min to minimize current facilitation (65) and the time-dependent change in deactivation (66). We saw no use-dependent change in *Pf*%, and therefore multiple determinations were averaged to yield a single value.

As noted above, the *Pf*% method requires that all the Ca^{2+} that enters the cell is captured by the high concentration of intracellular fura-2 (49). In most cases, this condition is satisfied using short applications of submaximal concentrations of agonist (1). The rat P2X7kR is an exception because its unusually slow deactivation produces sustained inward currents and Ca^{2+} fluxes (67, 68) that eventually saturate the intracellular fura-2. We found that the fura-2 remained unsaturated during the first 5–20 s of inward current because Ca^{2+} flux through the P2X7kR was unusually small (see below). Thus, all *Pf*% measurements of rat P2X7kRs are calculated from the initial, unsaturated portion of the response occurring in the first 20 s or less of the BzATP-gated inward current.

Calculating P_{Ca}/P_{Na}—We used our empirical measurements of *Pf*% to estimate P_{Ca}/P_{Na} using the following equation (54),

$$\frac{P_{Ca}}{P_{Na}} = \frac{\gamma_{Na} \times [Na]_o - \frac{P_{Cs}}{P_{Na}} \times \gamma_{Cs} \times [Cs]_i \times \exp\left(\frac{2VF}{RT}\right)}{4 \times \gamma_{Ca} \times [Ca]_o \times \left(\frac{1}{Pf} - 1\right)} \quad \text{(Eq. 1)}$$

where γ_{Na}, γ_{Cs}, and γ_{Ca} are the activity coefficients for Na^+ (0.72), Cs^+ (0.72), and Ca^{2+} (0.57), respectively. The concentrations of extracellular Na^+ and intracellular Cs^+ were those used in the *Pf*% experiments (see above), and the concentration of extracellular free Ca^{2+} was calculated using MaxChelator (69). P_{Cs}/P_{Na} equaled 1 (70). *F*, *R*, and *T* had their usual values at 22 °C, and *V* equaled −60 mV.

Measuring P_{NMDG}/P_{Na}—We used a standard reversal potential approach, described in detail in Migita *et al.* (71), to measure relative *N*-methyl-D-glucamine$^+$ ($NMDG^+$) permeability (*i.e.* P_{NMDG}/P_{Na}). Voltage ramps (140 mV, 200 ms) were applied

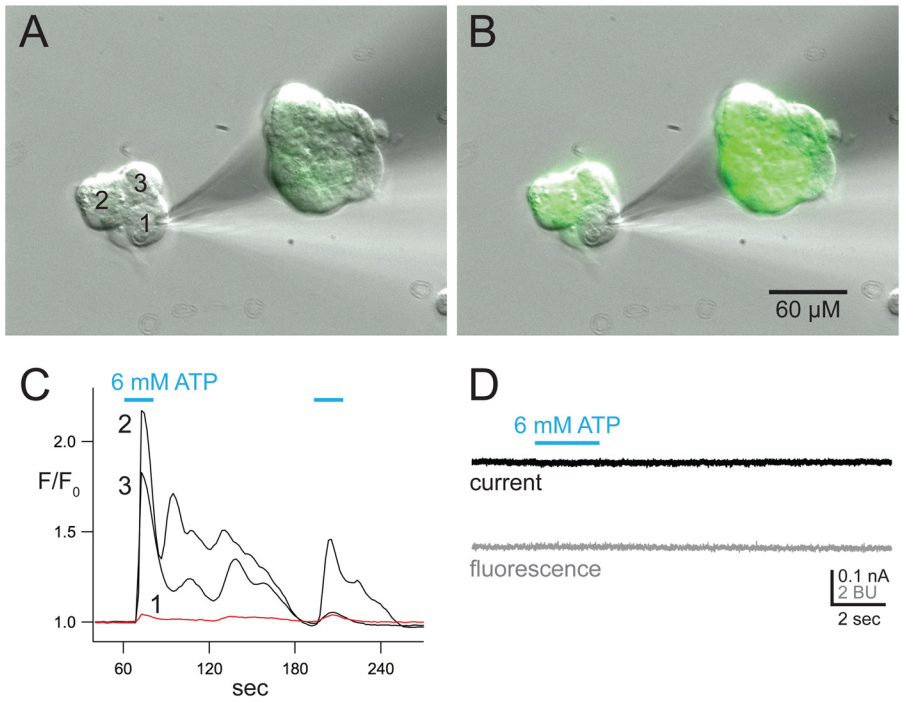

FIGURE 2. **The metabotropic P2Y response is missing in dialyzed cells.** *A*, resting HEK293-GCaMP5G cells show low levels of fluorescence. Cell *1* is undergoing internal dialysis with the contents of a recording electrode used for whole cell, broken-patch electrophysiology. The electrode contained the normal intracellular fura-2 solution used to measure *Pf*%. *B*, fluorescence increases dramatically in Cells *2* and *3* in response to activation of endogenous P2Y receptors by bath application of 6 mM ATP. The change in fluorescence intensity indicates an increase in $[Ca^{2+}]_i$. In contrast, Cell *1* shows no significant change in fluorescence. *C*, the change of fluorescence intensity was measured from each the three cells in the cluster. The image capture was started 5 min after the start of intracellular recording, and proceeded at a rate of one capture per 2 s. The change in fluorescence intensity was quantified by dividing the intensity of each capture by the average resting intensity measured before drug application. ATP was applied twice (*cyan bars*). *D*, current (*top*) and fura-2 F_{380} fluorescence (*bottom*) was captured from a single naive HEK293 using our standard method of measuring *Pf*%. ATP caused no measurable change in F_{380}. *BU*, bead units.

to HEK293 cells expressing P2X7Rs before and during short applications of BzATP (10–100 μM). The holding voltage was −100 mV, and the extracellular solution contained (in mM): 150 mM *X*Cl, 2 $CaCl_2$, 1 $MgCl_2$, 10 HEPES, and 10 glucose, pH 7.4, where *X* was either Na^+ or $NMDG^+$. Calcium and magnesium were included to replicate the conditions used to measure *Pf*%. The intracellular solution contained (in mM): 150 NaCl, 10 EGTA, 10 HEPES, pH 7.3. Relative $NMDG^+$ permeability (P_{NMDG}/P_{Na}) was determined from the difference in reversal potentials of agonist-gated currents measured in the two extracellular solutions ($\Delta E_{rev} = E_{rev,NMDG} - E_{rev,Na}$) as,

$$\frac{P_{NMDG}}{P_{Na}} = \frac{[Na]_i \times \gamma_{Na} \times \exp\left(\frac{\Delta E_{rev} F}{RT}\right) - 4 \times [Ca]_o \times \gamma_{Ca} \times \frac{P_{Ca}}{P_{Na}}}{[NMDG_o] \times \gamma_{NMDG}} \quad \text{(Eq. 2)}$$

where γ_{NMDG} equaled 0.72, and P_{Ca}/P_{Na} was calculated from the *Pf*% as described above (see Equation 1). ΔE_{rev} is the difference in reversal potentials measured in extracellular solutions containing either Na^+ and Ca^{2+} or $NMDG^+$ and Ca^{2+}.

Homology Modeling of Resting and Activated rP2X7aRs—Models for the rat P2X7 receptor were built as previously described (72). Briefly, the apo (Protein Data Bank 4DW0) and ATP-bound (Protein Data Bank 4DW1) structures of zP2X4.1 (73) were used as templates to generate the rP2X7aR models using the homology modeling server SWISSMODEL (74). The rP2X7aR models were minimized using the GROMOS force-field implemented in the program DEEP VIEW (75). Models were visualized in PyMol.

Data Analysis—We used GraphPad Prism for statistical analyses. The averaged values of pooled data with normal distributions are shown as mean ± S.E. Unless otherwise noted, groups were analyzed by one-way analysis of variance with significance determined by Tukey's multiple comparison test. The exceptions were analyzed using Student's *t* test. *p* values of ≤ 0.01 were considered statistically significant.

RESULTS

HEK293 cells express metabotropic P2Y receptors capable of increasing the concentration of intracellular Ca^{2+} ($[Ca^{2+}]_i$) by mobilizing internal Ca^{2+} stores in a GTP-dependent manner (76, 77). We used a HEK293 cell line with stable expression of the genetically encoded Ca^{2+} sensor, GCaMP5G (78), to determine whether activation of P2Y receptors by ATP (6 mM) is an unintended consequence of using high agonist concentrations to measure *Pf*%. We found that ATP increases $[Ca^{2+}]_i$ in unperturbed cells, but failed to do so in cells whose cytoplasm is dialyzed with the contents of a whole cell recording electrode (Fig. 2, *A–C*). Furthermore, when using our standard method of measuring *Pf*%, we saw no change in fura-2 fluorescence in mock transfected cells ($n = 11$) in response to a concentration of agonist (6 mM) that was 10–60 times higher than that applied to functional recombinant P2X7Rs in our study (Fig. 2*D*). These data support the contention that the internal dialysis that occurs during whole cell *Pf*% recordings disrupts the

TABLE 1

Measured and adjusted *Pf*% values

Pf% was measured from HEK293 cells expressing the specific P2X7R listed in the leftmost column. Concentrations are mM. Species are homomeric "a" splice variants unless otherwise noted in parentheses. 0.1 mM BzATP was dissolved in an extracellular solution containing 2 mM $CaCl_2$ and 1 mM $MgCl_2$. 0.6 mM BzATP was dissolved in an extracellular solution containing 2 mM $CaCl_2$ and no added $MgCl_2$. The estimated concentrations of free Ca^{2+} and Mg^{2+} were calculated using MaxChelator. $Pf\%_{adj}$ is the fractional Ca^{2+} current expected if *Pf*% could be measured in the absence of Ca^{2+} chelation by the purinergic agonist. P_{Ca}/P_{Na} was calculated from the empirically measured *Pf*% values as described under "Experimental Procedures."

Species	[BzATP]	$[Ca^{2+}]_{free}$	$[Mg^{2+}]_{free}$	*Pf*%	$Pf\%_{adj}$	P_{Ca}/P_{Na}	*n*
Dog	0.1	1.95	0.95	7.3 ± 0.2	7.5 ± 0.2	1.8 ± 0.0	11
Rat	0.1	1.95	0.95	7.1 ± 0.2	7.3 ± 0.2	1.7 ± 0.1	136
Rat (k)	0.1	1.95	0.95	2.8 ± 0.3[a]	2.8 ± 0.3[a]	0.7 ± 0.1[a]	34
Mouse	0.1	1.95	0.95	7.1 ± 0.4	7.3 ± 0.4	1.7 ± 0.1	11
Mouse (k)	0.1	1.95	0.95	4.3 ± 0.3[b]	4.4 ± 0.3[b]	1.0 ± 0.1[b]	13
Guinea pig	0.6	1.40	0	5.7 ± 0.8	8.2 ± 1.1	1.9 ± 0.3	7
Monkey	0.6	1.40	0	8.0 ± 0.4	11.4 ± 1.0	2.7 ± 0.3	8
Human	0.6	1.40	0	7.1 ± 0.4	10.2 ± 0.6	2.4 ± 0.2	22
Human X7 (a/b)	0.6	1.40	0	8.2 ± 0.3	11.7 ± 0.4	2.9 ± 0.1	8
Zebrafish	0.6	1.40	0	14.3 ± 1.0[c]	20.4 ± 1.4[c]	5.6 ± 0.5[c]	14

[a] Significantly different from rP2X7aR.
[b] Significantly different from mP2X7aR.
[c] Significantly different from all other species.

P2Y response (1). Confident that we could record a pure ionotropic response, we then moved to the study of the P2X7Rs.

Genes encoding the P2X7aRs of dog, frog, guinea pig, human, monkey, mouse, rat, and zebrafish were individually expressed in HEK293 cells for study using patch-clamp photometry. Cells expressing transfected genes were visually identified by the fluorescence emitted from a reporter protein (eGFP or dsRed), and the *Pf*% was determined as described above. Transfected cells responded with robust inward currents (membrane holding potential = −60 mV) and changes in fura-2 fluorescence to applications of BzATP (100–600 μM) with one exception: we failed to record agonist-gated current or a change in fura-2 fluorescence in response to BzATP (up to and including 1 mM) and ATP (6 mM) in HEK293 cells transfected with the gene encoding the *Xenopus laevis* P2X7aR. This was surprising because injection of frog P2X7aR cRNA results in large ATP-gated currents in a *Xenopus* oocyte expression system (79).

Most P2X7aRs Transduce Substantial Ca^{2+} Currents—In all other cases, we reliably measured the *Pf*% with the dye-overload technique. First, we tested the P2X7aR constructs using a concentration of BzATP (100 μM) that does not significantly chelate Ca^{2+} (estimated free $[Ca^{2+}]_o$ equaled 1.95 mM) (8). Only three (mouse, rat, and dog) of the seven responded with sizable membrane currents and changes in fura-2 fluorescence. In each case, the average *Pf*% equaled ~7% (Table 1). For the mouse ortholog, we studied both the Pro^{451} and Leu^{451} alleles (80, 81), and found no significant difference in their *Pf*% values.

Next, we used a higher concentration of BzATP (600 μM) and a Mg^{2+}-free test solution (9, 48) to elicit responses from the remaining four constructs (zebrafish, guinea pig, monkey, and human). Under these conditions, the calculated free $[Ca^{2+}]_o$ drops from 1.95 to 1.40 mM as the [BzATP] rises from 0.1 to 0.6 mM and the $[Mg^{2+}]_o$ falls from 1.0 to 0.0 mM. Although less Ca^{2+} was available to carry the agonist-gated current, we still measured substantial *Pf*% values equal to ~6–8% for guinea pig, monkey, and human P2X7aRs (Table 1). The *Pf*% of the zebrafish P2X7R was higher still at 14.3 ± 1.0% (n = 14).

Pf% Adjusted for Changes in $[Ca^{2+}]_o$—We sought to determine a fair method of comparing *Pf*% values measured under conditions where the free $[Ca^{2+}]_o$ varied as a consequence of the agonist concentration. To this end, we measured the *Pf*% values of rat P2X7aR currents elicited by 100 μM BzATP and a range of ATP concentrations (Fig. 3, *A* and *B*). We used ATP because the cost of using millimolar concentrations of BzATP was prohibitive, and because others have shown that ATP and BzATP bind Ca^{2+} equally well (8). Furthermore, ATP is the endogenous agonist for native receptors, and thus provides insight regarding the amplitude of the Ca^{2+} flux under pathophysiological conditions where the high $[ATP]_o$ causes significant buffering of extracellular Ca^{2+}. We calculated the extracellular concentration of free Ca^{2+} in a given concentration of BzATP or ATP using MaxChelator (Fig. 3*C*), and then empirically determined the *Pf*%. As expected, the *Pf*% progressively decreased with increasing concentrations of agonist (Fig. 3*D*), falling from a high of 7.1 ± 0.2% (n = 136) at 0.1 μM BzATP to a low of 1.7 ± 0.3% (n = 12) at 6 mM ATP. The XY-plot of *Pf*% *versus* free $[Ca^{2+}]_o$ was linear (Pearson's r = 0.99) with a slope of 3.8% per mM extracellular Ca^{2+} (Fig. 3*E*).

We took advantage of this linear relationship to calculate an adjusted *Pf*% ($Pf\%_{adj}$) equal to the product of *Pf*% and *R*, where *R* is the ratio of the free $[Ca^{2+}]_o$ values expected in the absence (2 mM) and presence of 100 or 600 μM BzATP. The $Pf\%_{adj}$ values are ~3 and 43% higher than the empirically measured *Pf*% values for 100 and 600 μM BzATP, respectively (Table 1), and thus represent the projected contribution of Ca^{2+} to the total agonist-gated cation current measured in the absence of Ca^{2+} chelation (Fig. 3*F*). We used a multiple comparisons test to detect differences among the mean $Pf\%_{adj}$ values of all seven species and found that one species differed from all others: that is, Ca^{2+} makes a greater adjusted contribution (~20%) to the BzATP-gated current of the zebrafish P2X7aR than it does in any other species. Indeed, the unadjusted, empirically determined *Pf*% measured in the relatively low $[Ca^{2+}]_o$ of 1.4 mM is still larger than that of other members of the ligand-gated ion channel superfamily measured in a higher $[Ca^{2+}]_o$ typically equal to 1.8 mM (82).

We investigated the cause of the transcendent *Pf*% of the zebrafish P2X7aR using a site-directed mutagenesis approach. The zebrafish P2X7aR retains the polar amino acids of TM2 that facilitate Ca^{2+} flux through rat P2X2Rs (1, 71), but lacks the vestibular acidic amino acids that are responsible for the high *Pf*% values of rat and human P2X1Rs and P2X4Rs (83, 84).

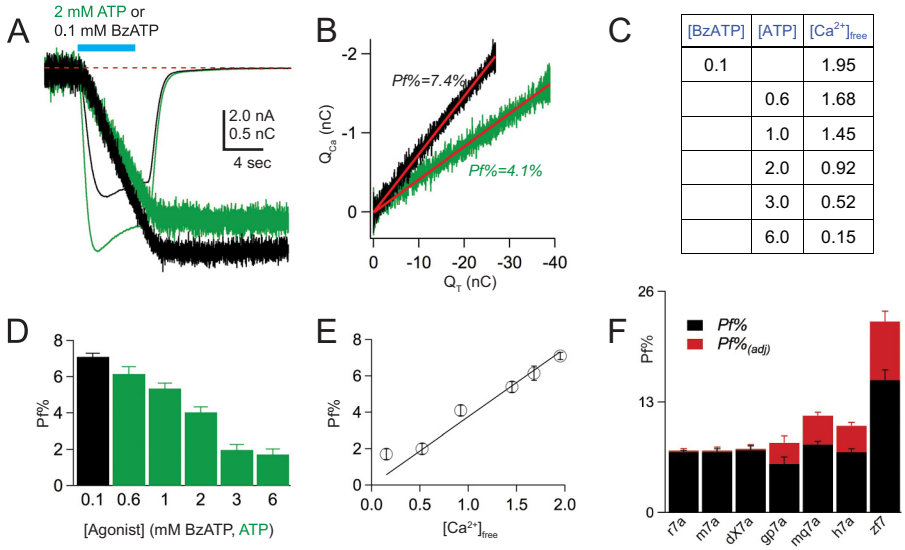

FIGURE 3. **Pf% decreases with increasing concentrations of ATP.** *A*, 2 mM ATP (*green traces*) evokes a larger current and smaller Q_{Ca} (shown in nC after conversion from bead units; see "Experimental Procedures") in an HEK293 cell expressing the rat P2X7aR than does 100 μM BzATP (*black traces*). *B*, the *Pf*%, determined from the linear fit of Q_{Ca} *versus* Q_T, is smaller for currents evoked by 2 mM ATP by comparison to 100 μM BzATP, despite the fact that the currents are larger. *C*, the calculated free $[Ca^{2+}]_o$ in different concentrations of BzATP and ATP. In these calculations, we used concentrations of total Na^+, Ca^{2+}, and Mg^{2+} equal to 150, 2, and 1 mM, respectively, a pH of 7.4, and a temperature of 23 °C. *D*, the histogram shows the average values ± S.E. of the *Pf*% of the rat P2X7aR measured using 100 μM BzATP (*black bar*) and increasing concentrations of ATP (*green bars*). The *Pf*% decreases with increasing concentrations of ATP. *E*, the graph plots empirical *Pf*% against the calculated free $[Ca^{2+}]_o$. The result is a straight line, suggesting that the decrease in *Pf*% reflects chelation of extracellular Ca^{2+} by the purinergic agonists. *F*, the histogram shows the *Pf*% (*black bars*) and *Pf*%$_{adj}$ (*red bars*) for a range of P2X7Rs.

We considered the possibility that two glutamates (Glu^{48} and Glu^{51}) just downstream of the zebrafish TM1 might take the place of the vestibular acidic amino acids of rat and human P2X1R and P2X4R that are missing in the P2X7Rs, and thus provide an electrostatic potential capable of concentrating Ca^{2+} at the entrance to the pore. To test this hypothesis, we removed the negative charge by mutating both glutamates to glutamine. Although the resulting mutant (zfP2X7aR-E48N/E51N) showed currents in response to 600 μM BzATP that were comparable in size to that of the wild-type zfP2X7R, the concomitant change in fluorescence was reduced. From these data, we calculated a *Pf*% equal to 8.0 ± 0.5% (n = 8), which is significantly smaller than that of the wild-type zebrafish receptor (~14%) and more in line with those of the other P2X7aR orthologs. This result suggests that acidic amino acids play a role in regulating the Ca^{2+} flux of the zfP2X7aR, perhaps by pulling Ca^{2+} into the lateral portals that form the entrance to the pore (72).

Co-transfection of hP2X7aR and hP2X7bR—Heteromeric hP2X7a/bRs show channel properties in fluorescent assays that differ from those of the homomeric hP2X7aR (56). To determine whether heteromerization affects Ca^{2+} transport, we measured the *Pf*% of the BzATP-gated current of HEK293 cells transfected with genes encoding P2X7aRs and hP2X7bRs. Cells expressing only the P2X7bR showed small membrane currents (<2 pA/pF) in response to relatively high concentrations of BzATP (600 μM) and ATP (6 mM). The fluorescent signals associated with these currents were too small to quantify. In contrast, 600 μM BzATP evoked large currents (>50 pA/pF) in cells co-transfected with a 1:3 ratio of the *hP2X7A* and *hP2X7B* genes. These currents resembled in size and shape those recorded from cells expressing only the hP2X7aR. We compared the ATP concentration-current curves of cells transfected with one or both genes to gauge heteromerization using a low-divalent (0.2 Ca^{2+} and no Mg^{2+}) extracellular solution (8, 9). In keeping with Adinolfi *et al.* (56), we saw leftward shifts in the concentration-current curves of cells transfected with both genes by comparison to cells expressing only the P2X7aR (Fig. 4). From these data, we measured a significant difference (Student's t test; $p < 0.01$) in agonist potency of cells transfected with one (hP2X7A; ATP EC_{50} = 5.3 ± 1.4 mM, n = 6) or both

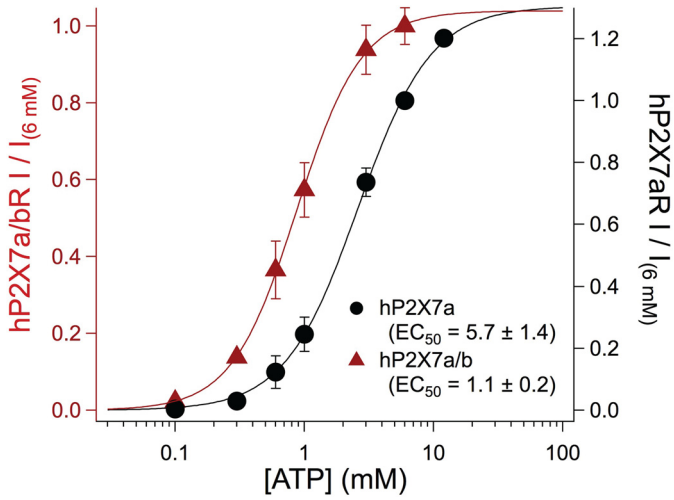

FIGURE 4. **Concentration-current curves for homomeric and heteromeric human P2X7Rs.** Concentration-response curves were built from HEK293 transfected either with the hP2X7aR plasmid alone (*black*), or co-transfected with the hP2X7aR and hP2X7bR plasmids (*red*). Each data point was normalized to the peak current caused by applying 6 mM ATP to the same cell. Individual data points corresponding to specific concentrations of ATP were averaged (*solid circles*). The *solid lines* show the best fit of the averaged data to the Hill equation. For statistical analysis, EC_{50} values were calculated from data of complete concentration-response curves obtained from 12 individual cells. Significance was determined using Student's t test.

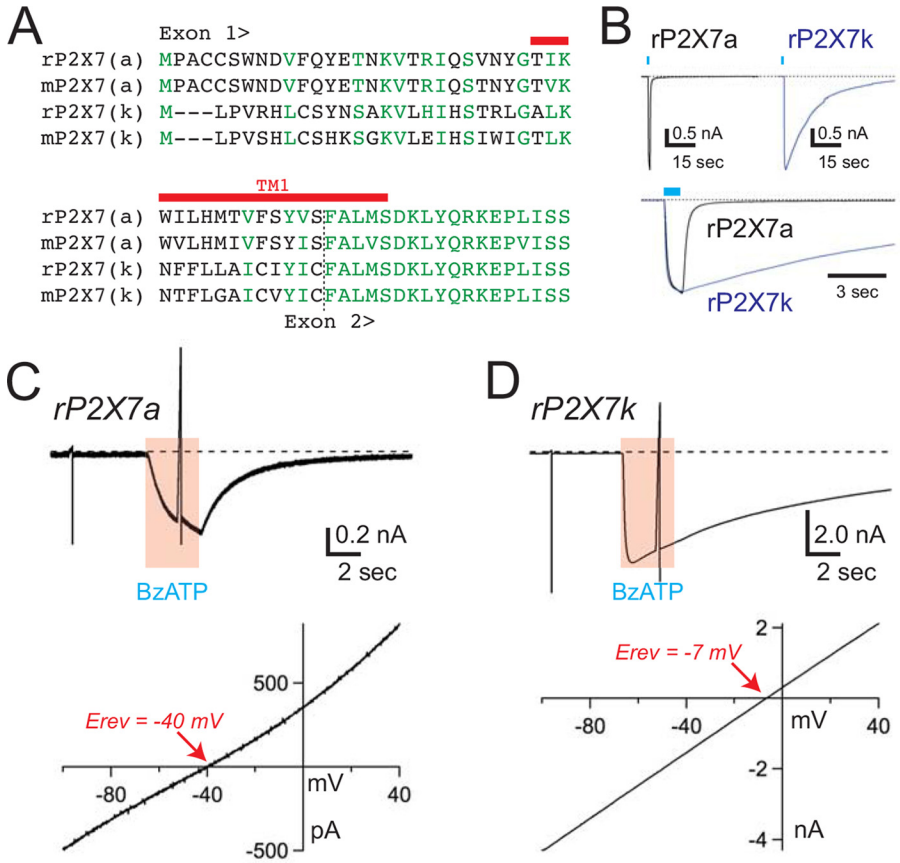

FIGURE 5. **The rP2X7kR is constitutively dilated.** *A*, sequence alignment of the N terminus and TM1 of rat and mouse P2X7a and P2X7k receptors. Identical and similar residues are shown in *green*. TM1 is marked with a *red bar*. *B*, the *top two traces* show the time courses of the membrane currents gated by 100 μM BzATP in voltage-clamped HEK293 cells (holding voltage = −60 mV) expressing either rP2X7aRs (*left*) or rP2X7kRs (*right*). The rP2X7kR often took several minutes to fully deactivate upon washout of agonist. In the *bottom trace*, normalized rP2X7aR and rP2X7kR currents are overlaid to show the difference in deactivation times. *C* and *D*, voltage ramps (140 mV, 200 ms) from a holding voltage of −100 mV were applied to HEK293 cells expressing either rP2X7aRs (*panel C*) or rP2X7kRs (*panel D*) before and during applications of 30 μM BzATP. Currents through the rP2X7aR were reversed at membrane potentials (*bottom left trace*) that were significantly more negative than the currents through the rP2X7kR (*bottom right trace*). These data support the hypothesis that the pore of the rP2X7kR is constitutively dilated. Similar results were found using the mouse splice variants.

(*hP2X7A*/*hP2X7B*; ATP EC_{50} = 1.1 ± 0.2 mM, n = 6) genes, suggesting that some of the agonist-gated current flows through a population of heteromeric receptors. We then measured the *Pf*% of cells co-transfected with genes encoding hP2X7aRs and hP2X7bRs. Although the *Pf*% values measured from these cells tended to be higher (8.2 ± 0.5%, n = 8) than cells expressing P2X7aR alone (~7.1%; see Table 1), the difference in the two values failed to reach statistical significance (Student's t test; p = 0.1229). Although many factors can influence the outcome of co-expression experiments, our results suggest that heteromerization affects the binding/gating properties of human P2X7Rs (*i.e.* the EC_{50}) more than ionic selectivity (*i.e.* the *Pf*%).

The Murine P2X7k Splice Variant Shows Limited Ca^{2+} Flux—Rat and mouse P2X7kRs are derived from an alternative exon 1′ (6) and contain unique N termini and TM1s that differ from those of the P2X7aR splice variants (Fig. 5*A*). We determined the *Pf*% values of the P2X7kR splice variants in response to the same concentration of BzATP (100 μM) used to study the P2X7aRs. We studied the rat P2X7kR first, and in keeping with previous reports (57), we found two obvious differences in the character of its BzATP-gated currents. First, deactivation of the transmembrane current was noticeably slower than that of the rat P2X7aR (Fig. 5*B*). Second, the reversal potential of the BzATP-gated current measured in an extracellular solution containing 150 mM $NMDG^+$, 2 mM Ca^{2+}, and 1 mM Mg^{2+} was right-shifted by ~25 mV (-41.8 ± 0.6 mV for the rP2X7aR, and −15.0 ± 2.4 mV for the rat P2X7kR; Fig. 5, *C* and *D*). These data yield P_{NMDG}/P_{Na} of 0.12 ± 0.00 (n = 12) and 0.55 ± 0.05 (n = 8) for the rat P2X7aR and P2X7kR, respectively. A similar difference was found for the mouse P2X7aR and P2X7kR (P_{NMDG}/P_{Na} 0.05 ± 0.01, n = 11; and 0.40 ± 0.03, n = 11). The disparity in baseline permeability to the large (4.5 Å) polyatomic $NMDG^+$ supports the suggestion that the selectivity filters of the P2X7a and P2X7k splice variants adopt different initial open state conformations with dissimilar cation permeabilities (57). To explore this hypothesis further, we sought to determine whether the contribution of the physiologically relevant divalent cation, Ca^{2+}, to whole cell current also differed.

We measured the *Pf*% of the BzATP-gated current of the rat and mouse P2X7kRs. In both instances, 100 μM BzATP evoked inward membrane currents and changes in fura-2 fluorescence emission as expected for non-selective cation channels permeable to Ca^{2+} (for example, see Fig. 6*A*). Within the constraints outlined under "Experimental Procedures," we measured a linear relationship of Q_{Ca} *versus* Q_T (Fig. 6*B*), as expected if all of

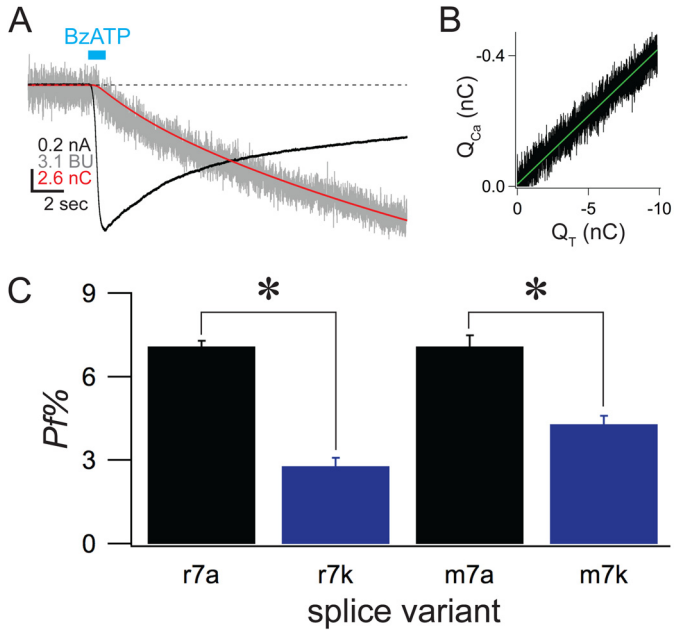

FIGURE 6. **The rP2X7kR carries a small Ca^{2+} current.** *A*, the traces show raw data of an experiment that measured the *Pf*% of a cell expressing the rP2X7kR. The cell was held at −60 mV under voltage-clamp. BzATP (100 μM) was applied for the time indicated by the *cyan bar*. The *black trace* is the membrane current measured in nAs. The *red trace* is the integrated membrane current and equals Q_T. The *gray trace* is the normalized fura-2 fluorescence, measured in bead units and proportional to Q_{Ca} (see "Experimental Procedures" for full details). *B*, the graph shows a linear relationship between Q_T (*x* axis) and fluorescence (*y* axis), a strict requirement of the dye-overload method (64). *C*, the histogram shows the average data of mouse and rat splice variants.

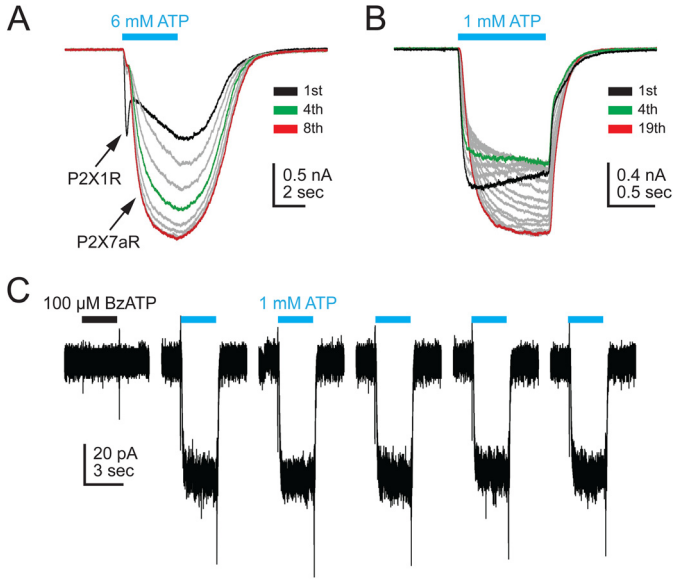

FIGURE 7. **Native currents of immune cells.** *A*, human macrophage. ATP was applied every 60 s for the time indicated by the *solid cyan bar*. The first application (*black trace*) shows a mixed response with P2X1R and P2X7aR components. Subsequent traces showed predominately P2X7aR currents. The P2X1R response was block by an antagonist during *Pf*% measurements (see "Results"). The P2X7aR response showed current facilitation similar to that described for many recombinant P2X7aRs. *Green* and *red traces* equal the fourth and eighth applications of ATP, respectively. *B*, mouse macrophage. The native response also showed facilitation. *C*, mouse regulatory T lymphocyte. 100 μM BzATP (*black bar*) had no effect on membrane current. In contrast, repetitive applications of ATP (1 mM) evoked steady currents that showed no facilitation.

the Ca^{2+} that binds to the intracellular fura-2 comes from the ATP-gated inward current traveling through the channel pore. We discovered that the *Pf*% of the agonist-gated inward current of the rat P2X7kR (2.8 ± 0.3%; $n = 34$) was significantly smaller than that of the rat P2X7aR (7.1%). Again, similar results were found when comparing splice variants from mouse (4.3 *versus* 7.1% for the P2X7kR and P2X7aR splice variants, respectively; see Fig. 6*C* and Table 1). Taken together, our measurements of P_{NMDG}/P_{Na} and *Pf*% show that P2X7kRs conduct smaller Ca^{2+} currents than rP2X7aRs despite having a higher permeability to large cations, implying that a critical Ca^{2+} selectivity filter is disrupted in the constitutively dilated P2X7kRs. These findings bring forth two intriguing hypotheses. First, P2X7a and P2X7k splice variants differ only in the composition of their N termini and TM1s. Their pore forming TM2 domains are identical, suggesting that they cannot be the primary sites responsible for the different *Pf*% of the two splice variants. Thus, our results suggest that domains that lie outside of the ion-conducting pathway of the P2X7R are capable of selectively regulating its Ca^{2+} current. Second, the physiologically relevant outcome of pore dilation may not be an increased permeability to large cations as generally assumed, but rather a decreased permeability to Ca^{2+}, an essential trigger of the downstream sequela of P2X receptor activation (5).

Relative Ca^{2+} Permeability—Relative Ca^{2+} permeabilities are commonly used to compare the selectivity of ligand-gated ion channels for Ca^{2+} (82, 85). Therefore, we used our empirical measurements of *Pf*% to estimate the relative Ca^{2+} to Na^+ permeability (P_{Ca}/P_{Na}) within the limits of the Goldman-Hodgkin-Katz equation (64), allowing the calcium selectivity of P2X7Rs to be compared with those of other P2XR subtypes and other classes of ligand-gated ion channels. The derived P_{Ca}/P_{Na} of the P2X7Rs equaled 0.7 to 5.6 (Table 1), values that approximate those of the empirically measured P_{Ca}/P_{Na} of other P2XR subtypes (1.2–4.8) and other ligand-gated channels (0.4–10.4) (82, 86, 87). As expected, the upper and lower limits of the purinergic P_{Ca}/P_{Na} were set by the zfP2X7aR and the murine P2X7kRs, respectively.

The Pf% of Native P2X7 Channels of Mouse and Human Immune Cells—We determined the *Pf*% of the BzATP-gated current of monocyte-derived macrophages isolated from mouse peritoneum and human blood (Fig. 7, *A* and *B*). After a minimum of 6 days in culture, we incubated the macrophages with 1 μg/ml of lipopolysaccharide for 6–12 h and then measured their response to 100 (mouse) or 600 μM (human) BzATP. The purinergic antagonist, 2′,3′-*O*-(2,4,6-trinitrophenyl)-ATP (100 nM), was included in the superfusate at the time of the experiment to block the possible contribution of P2X1Rs to the BzATP-gated current (see Fig. 7*A*) (88). Measured in this way, the *Pf*% of the ATP-gated current of mouse and human macrophages equaled 8.8 ± 1.0 ($n = 7$) and 9.0 ± 0.5% ($n = 10$), respectively. We then used the empirical measurements to calculate $Pf\%_{adj}$ and P_{Ca}/P_{Na} values. For mouse macrophages, $Pf\%_{adj}$ equaled 9.0 ± 1.0% and P_{Ca}/P_{Na} equaled 2.3 ± 0.3%. For human macrophages, $Pf\%_{adj}$ and P_{Ca}/P_{Na} equaled 12.8 ± 0.8 and 3.3 ± 0.2%, respectively. Macrophages preferentially express the P2X7aR (68). In keeping with this observation, we found no statistically significant difference in the *Pf*% measured from recombinant P2X7aRs expressed in HEK293 cells and

those measured from the native ATP-gated responses of species-matched macrophages. To the best of our knowledge, these values are the first quantitative measures of the Ca^{2+} current of a native P2X7aR, and prove the hypothesis that P2X7Rs transduce significant Ca^{2+} currents in immune cells.

Finally, we measured the *Pf*% of the ATP-gated current of mouse $CD4^+Foxp3^-$ conventional and $CD4^+Foxp3^+$ regulatory T-lymphocytes that preferentially express the P2X7kR splice variant (68), using the same extracellular divalent cation concentrations (2 mM total Ca^{2+} and 1 mM total Mg^{2+}) used to study recombinant P2X7kRs. Both types of resting $CD4^+$ T-lymphocytes failed to respond to either 100 μM BzATP or 1 mM ATP; at these concentrations, both agonists fully activate P2X7kRs (57, 89). Likewise, activated conventional $CD4^+$ T cells did not respond to either agonist with inward current. In contrast, 1 mM ATP evoked inward current (5.0 ± 1.3 pA/pF; $n = 11$) in activated $CD4^+$ regulatory T cells with a *Pf*% of 5.2 ± 0.6% ($n = 9$). The adjusted $Pf\%_{adj}$ equaled 7.1 ± 0.6% (free $[Ca^{2+}]_o = 1.45$; see Fig. 2*C*), and the calculated P_{Ca}/P_{Na} equaled 1.8 ± 0.2. These same cells failed to respond to 100 μM BzATP (Fig. 7*C*). The inability of BzATP to induce membrane current when applied at a concentration greatly exceeding its EC_{50} (~8 μM; see (57)), and the unexpectedly high *Pf*%, argue against the involvement of homomeric P2X7kRs in the $CD4^+Foxp3^+$ regulatory T cell response.

DISCUSSION

The allosteric block of P2X7R current by extracellular divalent cations complicates direct P_{Ca}/P_{Na} measurements, making it difficult to judge the relative merit of this subfamily as a Ca^{2+} source by comparison to other P2XRs and the ligand-gated ion channel superfamily as a whole. We circumvented this problem by measuring the fractional contribution of Ca^{2+} to the total ATP-gated membrane current (*i.e.* the *Pf*%) using a true-to-life concentration of extracellular Ca^{2+} and an appropriate membrane potential of −60 mV (90, 91). We found that empirical measurements using recombinant receptors ranged from 3 to ~15% by comparison to the average *Pf*% of the P2X family as a whole (8.6 ± 0.8%; *red dotted line* of Fig. 8*A*). However, these comparisons are not without fault. This is because the P2X7Rs of guinea pig, monkey, human, and zebrafish required a concentration of BzATP (600 μM) that was high enough to significantly lower the concentration of free $[Ca^{2+}]_o$. We circumvented this problem by calculating a $Pf\%_{adj}$ that accounts for the variations in free $[Ca^{2+}]_o$, and found that P2X7aRs take their place beside the P2X1R and P2X4R as family members that show significant Ca^{2+} currents. In contrast, the P2X7kRs, with the *Pf*%s (and $Pf\%_{adj}$) of ~3–4%, resemble those of P2X3Rs and P2X5Rs in showing no appreciable preference (calculated $P_{Ca}/P_{Na} \leq 1$) for Ca^{2+} over Na^+.

By measuring *Pf*% values, we were able to estimate P_{Ca}/P_{Na}. Our calculated values ranged from ~1 for the entirely cation non-selective P2X7kRs, to ~2–6 for the P2X7aRs that preferentially transport Ca^{2+} (see Table 1). We calculated similar ratios (~2–3) for the native responses of mouse and human macrophages and lymphocytes. All of these values are comparable with those measured from other types of ligand-gated ion channels (82), but remarkably different from that (P_{Ca}/P_{Na} =

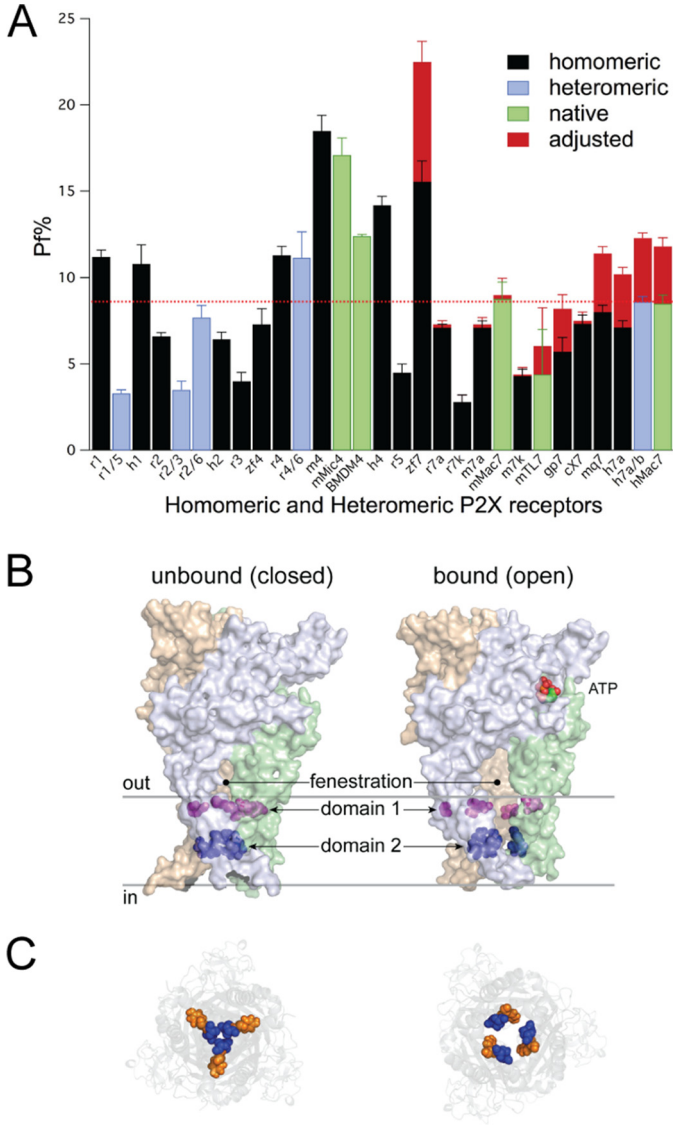

FIGURE 8. **Fractional Ca^{2+} current of homo- and heteromeric P2X receptors.** *A*, the graph shows the average *Pf*% for all homomeric (*black*), heteromeric (*blue*), and native (*green*) P2X receptors measured to date. Data of native and recombinant P2X7Rs come from the present study. Measures of the *Pf*% of recombinant P2X1R-P2X6Rs come from our published data (1, 83, 100) with one exception; data of recombinant hP2X2aR are previously unpublished observations. Data of the native P2X4R of mouse bone marrow-derived macrophages (*BMDM4*) are unpublished observations of Samways and Egan obtained during a previous study (27). The *red bars* indicate the average adjusted *Pf*% of the P2X7Rs expected in the absence of Ca^{2+} chelation by BzATP. The *red line* indicates the average *Pf*% of all P2XRs. P2X7R data come from the present study. *c*, *gp*, *h*, *m*, *mq*, *r*, and *zf* are canine, guinea pig, human, mouse, macaque, rat, and zebrafish data, respectively. *mMic4* are native currents of mouse microglia. *hMac7* and *mMac7* are native currents of human and mouse macrophages, respectively. *mTL7* are native currents of mouse $CD4^+Foxp3^+$ regulatory T lymphocytes. *B*, homology model of the closed and open truncated rat P2X7aR in the closed and open states viewed from the plane of the membrane. The cytoplasmic N and C termini are missing. The *solid gray lines* indicate the inner and outer limits of the membrane. *C*, view from inside the cell looking out. The panel shows how Domain-2 (Ser^{339}, Ser^{342} (*blue*), and Tyr^{343} (*orange*)) form a narrow corridor that widens during opening. The distance between these residues is expected to increase further during pore dilation, which might lead to disruption of a low-affinity Ca^{2+} binding site.

35) reported in an early study (92) of the unclassified (but presumably P2X7R-mediated) ATP-gated current of transformed human B-lymphocytes. Although it is possible that this ATP-

gated current is unique, a more likely explanation is that the measurement reflects the inherent difficulties of determining relative Ca^{2+} permeability using low concentrations of extracellular Ca^{2+} in cells expressing a P2X7R susceptible to allosteric block by divalent cations. Indeed, a P_{Ca}/P_{Na} of 35 translates to a *Pf*% of ~60%, which is unprecedented in the ligand-gated ion channel superfamily.

Using 1 mM ATP, we measured a $Pf\%_{adj}$ of ~7% from activated mouse $CD4^+Foxp3^+$ regulatory T cells, a value that is not significantly different from that of recombinant P2X7aRs expressed in HEK293 cells (also ~7%). This is surprising because these lymphocytes contain a 30-fold excess of P2X7kR mRNA by comparison to P2X7aR (68). At present, we do not know the identity of the receptor responsible for the regulatory T cell response. Although both the relatively large *Pf*% and the relatively low sensitivity to ATP suggest a P2X7aR response, the inability of 100 μM BzATP to induce current in cells that previously reacted to 1 mM ATP is unusual for either a P2X7aR or P2X7kR effect. One possibility is the contribution of a heteromeric receptor of undetermined components. Future biochemical, biophysical, and pharmacological studies are needed to determine whether this hypothesis is correct.

Our finding that the splice variants of the murine P2X7Rs differ almost 2-fold in *Pf*% suggests that structural regulation of the Ca^{2+} current is more complicated than previously imagined. Although definitive identification of the cation selectivity filter remains a work in progress (84), we previously documented two domains that contribute to the significant Ca^{2+} permeability and current of the P2XR family (Fig. 8*B*). "Domain 1" is made of juxtamembrane acidic amino acids (six in total in the trimeric receptor) that are present in family members with the highest *Pf*% (P2X1R, P2X4R), and either absent (P2X2R, P2X5R) or shielded (P2X3R) in members with lower *Pf*% values (83). Although the precise mechanism of action is unknown, we proposed that Domain 1 amino acids use the electrostatic attraction of COO^- side chains to concentrate Ca^{2+} in the fenestrae that form the entrance to the pore (84, 93). Our present results provide additional support for this hypothesis, as we now show that the very high *Pf*% of the zfP2X7R requires carboxylates at positions that are just extracellular to the transmembrane domains and expected to be in or near the mouth of the pore. Definitive proof of this hypothesis awaits the report of a high-resolution structural map of the zfP2X7R protein.

"Domain 2" is made of three polar amino acids (nine in total) that line the narrowest part of the rat P2X2R pore (see Fig. 8*B*). Others and we showed that altering the hydrophobicity, volume, and/or charge of residues in Domain 2 affect cation (71) and anion permeability (94), and *Pf*% (1). Sequence conservation in this domain is relatively poor, and whereas it seems likely that such a narrow part of the pore affects permeability and conduction across the entire family, additional experiments are needed to prove this hypothesis (84). Interestingly, the critical polar amino acids of the P2X2R (Thr^{336}, Thr^{339}, Ser^{340}) are conserved in all the P2X7Rs used in the present study, and a specific mutation of at least one of these (Ser^{342} of the rat P2X7aR, equivalent to Thr^{339} of the rat P2X2R) results in a loss-of-function (95).

Now, our experiments suggest that a third domain should also be considered. Murine P2X7aRs and P2X7kRs have identical pore forming TM2s but divergent *Pf*%, and differ only in the primary sequences of their N termini and TM1s. Site-directed mutagenesis of the TM1 of the rat P2X2R affects gating (96, 97) to a greater extent than the *Pf*% (62), suggesting that TM1 plays little or no role in modulation of the Ca^{2+} component of the ATP-gated current. We assume that this condition holds true for P2X7Rs too, and we plan to test this hypothesis in future experiments. If true, then the N terminus must be the site responsible for the different *Pf*% values of the two splice variants. Mutagenesis of the rat P2X7aR N terminus affects the conformational changes that accompany "pore dilation," a process by which a limiting constriction in the pore widens to the extent that large cations like $NMDG^+$ show appreciable permeability (65, 95, 98). We suggest that dilation of the pore results in disruption of the putative Domain 2 Ca^{2+} selectivity filter. In this scenario, Domain 2 is made of the side chains (or backbone carbonyl oxygens) of critical polar amino acids (for example, Ser^{339} and Ser^{342} of the rat P2X7aR) that loosely coordinate partially dehydrated Ca^{2+} and thereby facilitate Ca^{2+} transport through the pore. This binding site is disrupted in the constitutively dilated P2X7kRs where the distance between the polar amino acids is too great to provide the electrostatic potential needed to selectively bind Ca^{2+} at the expense of Na^+ and K^+. In 2004, Fisher *et al.* (99) speculated that pore dilation could alter the preferential flow of one ion over another, and our results support this proposition.

This said, we cannot rule out the possibility that pore dilation and regulation of the Ca^{2+} current are unrelated processes controlled by distinct domains, and that the co-occurrence of constitutive pore dilation and limited Ca^{2+} flux in the P2X7kR is coincidental. One way to address this issue is to study both processes in a single cell before and after onset of pore dilation, which might be possible for cells expressing the rat P2X7aR. Unfortunately, significant pore dilation measured in physiological concentrations of divalent cations requires a prolonged agonist exposure that results in a progressive leak of fura-2 out of the cell and Ca^{2+} into the cell (98); the unintended result is a saturation of the remaining fluorescent dye that negates the accuracy of the *Pf*% measurement. Future experiments on mutant P2X7aRs with altered pore properties may help to determine whether one or more structural domains underlie genesis of these two effects.

In conclusion, we show that P2X7aRs transduce a significant Ca^{2+} flux that is as large or larger than those of most ligand-gated channel families. In contrast, the constitutively dilated P2X7kRs show no selective preference for Ca^{2+}, which most likely reflects an N-terminal directed change in the conformation of the conducting pore. The results bring to light the intriguing hypothesis that the physiological consequence of pore dilation is a decrease in Ca^{2+} entry (99). Such a mechanism may have evolved to prevent Ca^{2+} overload in cells expressing P2X7aRs that show a time-dependent facilitation of peak current amplitude, or in cells expressing P2X7kRs with altered channel kinetics and/or increased sensitivities to ATP. Our data also demonstrate an important and somewhat overlooked physiological consequence of the substantial buffering

of Ca^{2+} at the high $[ATP]_o$ values that accompany disease. That is, elevated levels of extracellular ATP lead to smaller than expected Ca^{2+} currents, which would blunt agonist-gated responses triggered by an elevation of intracellular $[Ca^{2+}]$. At the same time, the reduction of $[Ca^{2+}]_o$ by ATP would partially relieve the allosteric Ca^{2+} block of the P2X7R, leading to a larger than expected peak current. In the future, it will be important to consider all of these factors when attempting to gauge the likely response of any cell expressing a P2X7R to ATP.

Acknowledgments—We thank Drs. Elena Adinolfi, Lin-Hua Jiang, Stefan Gründer, Annette Nicke, Richard Alan North, Ronald Sluyter, Stanko Stojilkovic, and Mark Voigt for supplying P2X7R plasmids. We also thank Drs. Randy Sprague and Timothy Doyle for help in isolating human macrophages, Dr. Floretina Soto for critiquing a pre-submission version of the manuscript, and Dr. Donald Bers for useful discussions and initial calculations of the Ca^{2+} buffering capacity of ATP in defined extracellular solutions.

REFERENCES

1. Egan, T. M., and Khakh, B. S. (2004) Contribution of calcium ions to P2X channel responses. *J. Neurosci.* **24,** 3413–3420
2. North, R. A., and Jarvis, M. F. (2013) P2X receptors as drug targets. *Mol. Pharmacol.* **83,** 759–769
3. Burnstock, G., and Kennedy, C. (2011) P2X receptors in health and disease. *Adv. Pharmacol.* **61,** 333–372
4. Jiang, L.-H. (2012) P2X receptor-mediated ATP purinergic signaling in health and disease. *Cell Health Cytoskeleton* **4,** 83–101
5. Khakh, B. S., and North, R. A. (2012) Neuromodulation by Extracellular ATP and P2X Receptors in the CNS. *Neuron* **76,** 51–69
6. Kaczmarek-Hájek, K., Lörinczi, E., Hausmann, R., and Nicke, A. (2012) Molecular and functional properties of P2X receptors: recent progress and persisting challenges. *Purinergic Signal.* **8,** 375–417
7. Jiang, R., Taly, A., and Grutter, T. (2013) Moving through the gate in ATP-activated P2X receptors. *Trends Biochem. Sci.* **38,** 20–29
8. Yan, Z., Khadra, A., Sherman, A., and Stojilkovic, S. S. (2011) Calcium-dependent block of P2X7 receptor channel function is allosteric. *J. Gen. Physiol.* **138,** 437–452
9. Virginio, C., Church, D., North, R. A., and Surprenant, A. (1997) Effects of divalent cations, protons and calmidazolium at the rat P2X7 receptor. *Neuropharmacology* **36,** 1285–1294
10. Jiang, L. H. (2009) Inhibition of P2X(7) receptors by divalent cations: old action and new insight. *Eur. Biophys. J.* **38,** 339–346
11. Collo, G., Neidhart, S., Kawashima, E., Kosco-Vilbois, M., North, R. A., and Buell, G. (1997) Tissue distribution of the P2X7 receptor. *Neuropharmacology* **36,** 1277–1283
12. Di Virgilio, F., Ceruti, S., Bramanti, P., and Abbracchio, M. P. (2009) Purinergic signalling in inflammation of the central nervous system. *Trends Neurosci.* **32,** 79–87
13. Surprenant, A., and North, R. A. (2009) Signaling at purinergic P2X receptors. *Annu. Rev. Physiol.* **71,** 333–359
14. Grol, M. W., Panupinthu, N., Korcok, J., Sims, S. M., and Dixon, S. J. (2009) Expression, signaling, and function of P2X7 receptors in bone. *Purinergic Signal.* **5,** 205–221
15. Chen, L., and Brosnan, C. F. (2006) Regulation of immune response by P2X7 receptor. *Crit. Rev. Immunol.* **26,** 499–513
16. Gordon, J. L. (1986) Extracellular ATP: effects, sources and fate. *Biochem. J.* **233,** 309–319
17. Zimmermann, H. (2000) Extracellular metabolism of ATP and other nucleotides. *Naunyn Schmiedebergs Arch. Pharmacol.* **362,** 299–309
18. Di Virgilio, F., Boeynaems, J. M., and Robson, S. C. (2009) Extracellular nucleotides as negative modulators of immunity. *Curr. Opin. Pharmacol.* **9,** 507–513
19. Guerra, A. N., Gavala, M. L., Chung, H. S., and Bertics, P. J. (2007) Nucleotide receptor signalling and the generation of reactive oxygen species. *Purinergic Signal.* **3,** 39–51
20. Di Virgilio, F., Pizzo, P., Zanovello, P., Bronte, V., and Collavo, D. (1990) Extracellular ATP as a possible mediator of cell-mediated cytotoxicity. *Immunol. Today* **11,** 274–277
21. Lazarowski, E. R., Boucher, R. C., and Harden, T. K. (2000) Constitutive release of ATP and evidence for major contribution of ecto-nucleotide pyrophosphatase and nucleoside diphosphokinase to extracellular nucleotide concentrations. *J. Biol. Chem.* **275,** 31061–31068
22. Ogura, Y., Sutterwala, F. S., and Flavell, R. A. (2006) The inflammasome: first line of the immune response to cell stress. *Cell* **126,** 659–662
23. Sutterwala, F. S., Ogura, Y., Szczepanik, M., Lara-Tejero, M., Lichtenberger, G. S., Grant, E. P., Bertin, J., Coyle, A. J., Galán, J. E., Askenase, P. W., and Flavell, R. A. (2006) Critical role for NALP3/CIAS1/Cryopyrin in innate and adaptive immunity through its regulation of caspase-1. *Immunity* **24,** 317–327
24. Di Virgilio, F. (2007) Liaisons dangereuses: P2X(7) and the inflammasome. *Trends Pharmacol. Sci.* **28,** 465–472
25. Skaper, S. D., Debetto, P., and Giusti, P. (2009) The P2X7 purinergic receptor: from physiology to neurological disorders. *FASEB J.* **24,** 337–345
26. Lister, M. F., Sharkey, J., Sawatzky, D. A., Hodgkiss, J. P., Davidson, D. J., Rossi, A. G., and Finlayson, K. (2007) The role of the purinergic P2X7 receptor in inflammation. *J. Inflamm.* **4,** 5
27. Scatizzi, J. C., Mavers, M., Hutcheson, J., Young, B., Shi, B., Pope, R. M., Ruderman, E. M., Samways, D. S., Corbett, J. A., Egan, T. M., and Perlman, H. (2009) The CDK domain of p21 is a suppressor of IL-1β-mediated inflammation in activated macrophages. *Eur. J. Immunol.* **39,** 820–825
28. Gudipaty, L., Munetz, J., Verhoef, P. A., and Dubyak, G. R. (2003) Essential role for Ca^{2+} in the regulation of IL-1β secretion by the P2X7 nucleotide receptor in monocytes, macrophages, and HEK293 fibroblasts. *Am. J. Physiol. Cell Physiol.* **285,** C286–C299
29. MacKenzie, A., Wilson, H. L., Kiss-Toth, E., Dower, S. K., North, R. A., and Surprenant, A. (2001) Rapid secretion of interleukin-1β by microvesicle shedding. *Immunity* **15,** 825–835
30. Qu, Y., Franchi, L., Nunez, G., and Dubyak, G. R. (2007) Nonclassical IL-1β secretion stimulated by P2X7 receptors is dependent on inflammasome activation and correlated with exosome release in murine macrophages. *J. Immunol.* **179,** 1913–1925
31. Hanley, P. J., Kronlage, M., Kirschning, C., del Rey, A., Di Virgilio, F., Leipziger, J., Chessell, I. P., Sargin, S., Filippov, M. A., Lindemann, O., Mohr, S., Königs, V., Schillers, H., Bähler, M., and Schwab, A. (2012) Transient P2X7 receptor activation triggers macrophage death independent of Toll-like receptors 2 and 4, caspase-1, and pannexin-1 proteins. *J. Biol. Chem.* **287,** 10650–10663
32. Glaser, T., Resende, R. R., and Ulrich, H. (2013) Implications of purinergic receptor-mediated intracellular calcium transients in neural differentiation. *Cell Commun. Signal.* **11,** 12
33. Sperlágh, B., Heinrich, A., and Csölle, C. (2007) P2 receptor-mediated modulation of neurotransmitter release-an update. *Purinergic Signal.* **3,** 269–284
34. Weisman, G. A., Camden, J. M., Peterson, T. S., Ajit, D., Woods, L. T., and Erb, L. (2012) P2 receptors for extracellular nucleotides in the central nervous system: role of P2X7 and P2Y(2) receptor interactions in neuroinflammation. *Mol. Neurobiol.* **46,** 96–113
35. Volonte, C., Apolloni, S., Skaper, S. D., and Burnstock, G. (2012) P2X7 receptors: channels, pores and more. *CNS Neurol. Discord. Drug Targets* **11,** 705–721
36. Köles, L., Leichsenring, A., Rubini, P., and Illes, P. (2011) P2 receptor signaling in neurons and glial cells of the central nervous system. *Adv. Pharmacol.* **61,** 441–493
37. Gulbransen, B. D., Bashashati, M., Hirota, S. A., Gui, X., Roberts, J. A., MacDonald, J. A., Muruve, D. A., McKay, D. M., Beck, P. L., Mawe, G. M., Thompson, R. J., and Sharkey, K. A. (2012) Activation of neuronal P2X7 receptor-pannexin-1 mediates death of enteric neurons during colitis. *Nat. Med.* **18,** 600–604
38. Notomi, S., Hisatomi, T., Murakami, Y., Terasaki, H., Sonoda, S., Asato,

R., Takeda, A., Ikeda, Y., Enaida, H., Sakamoto, T., and Ishibashi, T. (2013) Dynamic increase in extracellular ATP accelerates photoreceptor cell apoptosis via ligation of P2RX7 in subretinal hemorrhage. *PLoS One* **8,** e53338
39. Faroni, A., Rothwell, S. W., Grolla, A. A., Terenghi, G., Magnaghi, V., and Verkhratsky, A. (2013) Differentiation of adipose-derived stem cells into Schwann cell phenotype induces expression of P2X receptors that control cell death. *Cell Death Dis.* **4,** e743
40. Rubini, P., Pagel, G., Mehri, S., Marquardt, P., Riedel, T., and Illes, P. (2014) Functional P2X7 receptors at cultured hippocampal astrocytes but not neurons. *Naunyn Schmiedebergs Arch. Pharmacol.* **387,** 943–954
41. Deuchars, S. A., Atkinson, L., Brooke, R. E., Musa, H., Milligan, C. J., Batten, T. F., Buckley, N. J., Parson, S. H., and Deuchars, J. (2001) Neuronal P2X7 receptors are targeted to presynaptic terminals in the central and peripheral nervous systems. *J. Neurosci.* **21,** 7143–7152
42. Sperlágh, B., Vizi, E. S., Wirkner, K., and Illes, P. (2006) P2X7 receptors in the nervous system. *Prog. Neurobiol.* **78,** 327–346
43. Alloisio, S., Cervetto, C., Passalacqua, M., Barbieri, R., Maura, G., Nobile, M., and Marcoli, M. (2008) Functional evidence for presynaptic P2X7 receptors in adult rat cerebrocortical nerve terminals. *FEBS Lett.* **582,** 3948–3953
44. Marcoli, M., Cervetto, C., Paluzzi, P., Guarnieri, S., Alloisio, S., Thellung, S., Nobile, M., and Maura, G. (2008) P2X(7) pre-synaptic receptors in adult rat cerebrocortical nerve terminals: a role in ATP-induced glutamate release. *J. Neurochem.* **105,** 2330–2342
45. Sperlágh, B., Köfalvi, A., Deuchars, J., Atkinson, L., Milligan, C. J., Buckley, N. J., and Vizi, E. S. (2002) Involvement of P2X7 receptors in the regulation of neurotransmitter release in the rat hippocampus. *J. Neurochem.* **81,** 1196–1211
46. Cuadra, A. E., Custer, E. E., Bosworth, E. L., and Lemos, J. R. (2014) P2X7 receptors in neurohypophysial terminals: evidence for their role in arginine-vasopressin secretion. *J. Cell Physiol.* **229,** 333–342
47. Hille, B. (1992) Ionic channels of excitable membranes, 2nd Ed., p. 21, Sinauer Associates, Inc., Sunderland, MA
48. Stojilkovic, S. S., Leiva-Salcedo, E., Rokic, M. B., and Coddou, C. (2014) Regulation of ATP-Gated P2X channels: from redox signaling to interactions with other proteins. *Antioxid. Redox. Signal.* **21,** 953–970
49. Schneggenburger, R., Zhou, Z., Konnerth, A., and Neher, E. (1993) Fractional contribution of calcium to the cation current through glutamate receptor channels. *Neuron* **11,** 133–143
50. Rogers, M., and Dani, J. A. (1995) Comparison of quantitative calcium flux through NMDA, ATP, and ACh receptor channels. *Biophys. J.* **68,** 501–506
51. Partridge, L. D., Zeilhofer, H. U., and Swandulla, D. (1998) Combined whole-cell and single-channel current measurement with quantitative Ca^{2+} injection or Fura-2 measurement of Ca^{2+}. *Methods Enzymol.* **293,** 371–383
52. Zeilhofer, H. U., Swandulla, D., Reeh, P. W., and Kress, M. (1996) Ca^{2+} permeability of the sustained proton-induced cation current in adult rat dorsal root ganglion neurons. *J. Neurophysiol.* **76,** 2834–2840
53. Frings, S., Hackos, D. H., Dzeja, C., Ohyama, T., Hagen, V., Kaupp, U. B., and Korenbrot, J. I. (2000) Determination of fractional calcium ion current in cyclic nucleotide-gated channels. *Methods Enzymol.* **315,** 797–817
54. Jatzke, C., Watanabe, J., and Wollmuth, L. P. (2002) Voltage and concentration dependence of Ca^{2+} permeability in recombinant glutamate receptor subtypes. *J. Physiol.* **538,** 25–39
55. Wollmuth, L. P., and Sakmann, B. (1998) Different mechanisms of Ca2+ transport in NMDA and Ca^{2+}-permeable AMPA glutamate receptor channels. *J. Gen. Physiol.* **112,** 623–636
56. Adinolfi, E., Cirillo, M., Woltersdorf, R., Falzoni, S., Chiozzi, P., Pellegatti, P., Callegari, M. G., Sandonà, D., Markwardt, F., Schmalzing, G., and Di Virgilio, F. (2010) Trophic activity of a naturally occurring truncated isoform of the P2X7 receptor. *FASEB J.* **24,** 3393–3404
57. Nicke, A., Kuan, Y. H., Masin, M., Rettinger, J., Marquez-Klaka, B., Bender, O., Górecki, D. C., Murrell-Lagnado, R. D., and Soto, F. (2009) A functional P2X7 splice variant with an alternative transmembrane domain 1 escapes gene inactivation in P2X7 knock-out mice. *J. Biol. Chem.* **284,** 25813–25822
58. Nörenberg, W., Sobottka, H., Hempel, C., Plötz, T., Fischer, W., Schmalzing, G., and Schaefer, M. (2012) Positive allosteric modulation by ivermectin of human but not murine P2X7 receptors. *Br. J. Pharmacol.* **167,** 48–66
59. Davies, J. Q., and Gordon, S. (2005) Isolation and culture of murine macrophages. *Methods Mol. Biol.* **290,** 91–103
60. Lin, W., Haribhai, D., Relland, L. M., Truong, N., Carlson, M. R., Williams, C. B., and Chatila, T. A. (2007) Regulatory T cell development in the absence of functional Foxp3. *Nat. Immunol.* **8,** 359–368
61. Samways, D. S., Khakh, B. S., and Egan, T. M. (2012) Allosteric modulation of Ca^{2+} flux in ligand-gated cation channel (P2X4) by actions on lateral portals. *J. Biol. Chem.* **287,** 7594–7602
62. Samways, D. S., Migita, K., Li, Z., and Egan, T. M. (2008) On the role of the first transmembrane domain in cation permeability and flux of the ATP-gated P2X2 receptor. *J. Biol. Chem.* **283,** 5110–5117
63. Edelstein, A., Amodaj, N., Hoover, K., Vale, R., and Stuurman, N. (2010) Computer control of microscopes using microManager. *Current Protocols in Molecular Biology* 14.20.1–14.20.17, 10.1002/0471142727.mb1420s92
64. Neher, E. (1995) The use of fura-2 for estimating Ca buffers and Ca fluxes. *Neuropharmacology* **34,** 1423–1442
65. Surprenant, A., Rassendren, F., Kawashima, E., North, R. A., and Buell, G. (1996) The cytolytic P2Z receptor for extracellular ATP identified as a P2X receptor (P2X7). *Science* **272,** 735–738
66. Yan, Z., Khadra, A., Li, S., Tomic, M., Sherman, A., and Stojilkovic, S. S. (2010) Experimental characterization and mathematical modeling of P2X7 receptor channel gating. *J. Neurosci.* **30,** 14213–14224
67. Nicke, A. (2004) Learning about structure and function of neuronal nicotinic acetylcholine receptors: lessons from snails. *Eur. J. Biochem.* **271,** 2293
68. Schwarz, N., Drouot, L., Nicke, A., Fliegert, R., Boyer, O., Guse, A. H., Haag, F., Adriouch, S., and Koch-Nolte, F. (2012) Alternative splicing of the N-terminal cytosolic and transmembrane domains of P2X7 controls gating of the ion channel by ADP-ribosylation. *PLoS One* **7,** e41269
69. Bers, D. M., Patton, C. W., and Nuccitelli, R. (2010) A practical guide to the preparation of Ca^{2+} buffers. *Methods Cell Biol.* **99,** 1–26
70. Riedel, T., Schmalzing, G., and Markwardt, F. (2007) Influence of extracellular monovalent cations on pore and gating properties of P2X7 receptor-operated single-channel currents. *Biophys. J.* **93,** 846–858
71. Migita, K., Haines, W. R., Voigt, M. M., and Egan, T. M. (2001) Polar residues of the second transmembrane domain influence cation permeability of the ATP-gated P2X(2) receptor. *J. Biol. Chem.* **276,** 30934–30941
72. Samways, D. S., Khakh, B. S., Dutertre, S., and Egan, T. M. (2011) Preferential use of unobstructed lateral portals as the access route to the pore of human ATP-gated ion channels (P2X receptors). *Proc. Natl. Acad. Sci. U.S.A.* **108,** 13800–13805
73. Hattori, M., and Gouaux, E. (2012) Molecular mechanism of ATP binding and ion channel activation in P2X receptors. *Nature* **485,** 207–212
74. Schwede, T., Kopp, J., Guex, N., and Peitsch, M. C. (2003) SWISS-MODEL: an automated protein homology-modeling server. *Nucleic Acids Res.* **31,** 3381–3385
75. Guex, N., and Peitsch, M. C. (1997) SWISS-MODEL and the Swiss-PdbViewer: an environment for comparative protein modeling. *Electrophoresis* **18,** 2714–2723
76. He, M. L., Zemkova, H., Koshimizu, T. A., Tomic, M., and Stojilkovic, S. S. (2003) Intracellular calcium measurements as a method in studies on activity of purinergic P2X receptor channels. *Am. J. Physiol. Cell Physiol.* **285,** 467–479
77. Fischer, W., Wirkner, K., Weber, M., Eberts, C., Köles, L., Reinhardt, R., Franke, H., Allgaier, C., Gillen, C., and Illes, P. (2003) Characterization of P2X3, P2Y1 and P2Y4 receptors in cultured HEK293-hP2X3 cells and their inhibition by ethanol and trichloroethanol. *J. Neurochem.* **85,** 779–790
78. Akerboom, J., Chen, T. W., Wardill, T. J., Tian, L., Marvin, J. S., Mutlu, S., Calderón, N. C., Esposti, F., Borghuis, B. G., Sun, X. R., Gordus, A., Orger, M. B., Portugues, R., Engert, F., Macklin, J. J., Filosa, A., Aggarwal, A., Kerr, R. A., Takagi, R., Kracun, S., Shigetomi, E., Khakh, B. S., Baier, H., Lagnado, L., Wang, S. S., Bargmann, C. I., Kimmel, B. E., Jayaraman, V., Svoboda, K., Kim, D. S., Schreiter, E. R., and Looger, L. L. (2012) Optimi-

zation of a GCaMP calcium indicator for neural activity imaging. *J. Neurosci.* **32,** 13819–13840
79. Paukert, M., Hidayat, S., and Gründer, S. (2002) The P2X(7) receptor from *Xenopus laevis*: formation of a large pore in *Xenopus* oocytes. *FEBS Lett.* **513,** 253–258
80. Adriouch, S., Dox, C., Welge, V., Seman, M., Koch-Nolte, F., and Haag, F. (2002) Cutting edge: a natural P451L mutation in the cytoplasmic domain impairs the function of the mouse P2X7 receptor. *J. Immunol.* **169,** 4108–4112
81. Taylor, S. R., Gonzalez-Begne, M., Sojka, D. K., Richardson, J. C., Sheardown, S. A., Harrison, S. M., Pusey, C. D., Tam, F. W., and Elliott, J. I. (2009) Lymphocytes from P2X7-deficient mice exhibit enhanced P2X7 responses. *J. Leukocyte Biol.* **85,** 978–986
82. Pankratov, Y., and Lalo, U. (2013) Calcium permeability of ligand-gated Ca channels. *Eur. J. Pharmacol.* **739,** 60–73
83. Samways, D. S., and Egan, T. M. (2007) Acidic amino acids impart enhanced Ca^{2+} permeability and flux in two members of the ATP-gated P2X receptor family. *J. Gen. Physiol.* **129,** 245–256
84. Samways, D. S., Li, Z., and Egan, T. M. (2014) Principles and properties of ion flow in P2X receptors. *Front Cell Neurosci.* **8,** 6
85. Burnashev, N. (1996) Calcium permeability of glutamate-gated channels in the central nervous system. *Curr. Opin. Neurobiol.* **6,** 311–317
86. Burnashev, N. (1998) Calcium permeability of ligand-gated channels. *Cell Calcium* **24,** 325–332
87. Jarvis, M. F., and Khakh, B. S. (2009) ATP-gated P2X cation-channels. *Neuropharmacology* **56,** 208–215
88. Sim, J. A., Park, C. K., Oh, S. B., Evans, R. J., and North, R. A. (2007) P2X1 and P2X4 receptor currents in mouse macrophages. *Br. J. Pharmacol.* **152,** 1283–1290
89. Xu, X. J., Boumechache, M., Robinson, L. E., Marschall, V., Gorecki, D. C., Masin, M., and Murrell-Lagnado, R. D. (2012) Splice variants of the P2X7 receptor reveal differential agonist dependence and functional coupling with pannexin-1. *J. Cell Sci.* **125,** 3776–3789
90. Ozaki, H., Kawai, T., Shuttleworth, C. W., Won, K. J., Suzuki, T., Sato, K., Horiguchi, H., Hori, M., Karaki, H., Torihashi, S., Ward, S. M., and Sanders, K. M. (2004) Isolation and characterization of resident macrophages from the smooth muscle layers of murine small intestine. *Neurogastroenterol. Motil.* **16,** 39–51
91. Gallin, E. K., and McKinney, L. C. (1989) Ion Transport in Phagocytes. in *The Neutrophil: Cellular Biochemistry and Physiology* (Hallett, M. B., ed) pp. 243–260, CRC Press, Boca Raton, FL
92. Bretschneider, F., Klapperstück, M., Löhn, M., and Markwardt, F. (1995) Nonselective cationic currents elicited by extracellular ATP in human B-lymphocytes. *Pflugers Arch.* **429,** 691–698
93. Baconguis, I., Hattori, M., and Gouaux, E. (2013) Unanticipated parallels in architecture and mechanism between ATP-gated P2X receptors and acid sensing ion channels. *Curr. Opin. Struct. Biol.* **23,** 277–284
94. Browne, L. E., Cao, L., Broomhead, H. E., Bragg, L., Wilkinson, W. J., and North, R. A. (2011) P2X receptor channels show threefold symmetry in ionic charge selectivity and unitary conductance. *Nat. Neurosci.* **14,** 17–18
95. Browne, L. E., Compan, V., Bragg, L., and North, R. A. (2013) P2X7 receptor channels allow direct permeation of nanometer-sized dyes. *J. Neurosci.* **33,** 3557–3566
96. Torres, G. E., Egan, T. M., and Voigt, M. M. (1999) Identification of a domain involved in ATP-gated ionotropic receptor subunit assembly. *J. Biol. Chem.* **274,** 22359–22365
97. Jiang, L. H., Rassendren, F., Spelta, V., Surprenant, A., and North, R. A. (2001) Amino acid residues involved in gating identified in the first membrane-spanning domain of the rat P2X(2) receptor. *J. Biol. Chem.* **276,** 14902–14908
98. Yan, Z., Li, S., Liang, Z., Tomić, M., and Stojilkovic, S. S. (2008) The P2X7 receptor channel pore dilates under physiological ion conditions. *J. Gen. Physiol.* **132,** 563–573
99. Fisher, J. A., Girdler, G., and Khakh, B. S. (2004) Time-resolved measurement of state-specific P2X2 ion channel cytosolic gating motions. *J. Neurosci.* **24,** 10475–10487
100. Toulme, E., Garcia, A., Samways, D., Egan, T. M., Carson, M. J., and Khakh, B. S. (2010) P2X4 receptors in activated C8-B4 cells of cerebellar microglial origin. *J. Gen. Physiol.* **135,** 333–353